IEEE Access
Multidisciplinary | Rapid Review | Open Access Journal

Received 24 November 2022, accepted 12 December 2022, date of publication 15 December 2022,
date of current version 22 December 2022.

Digital Object Identifier 10.1109/ACCESS.2022.3229686

RESEARCH ARTICLE

Simulation and Fabrication of Micro-Electrode Arrays for Electrical Stimulation Induced Wound Healing

G. HARISH GNANASAMBANTHAN AND DEBASHIS MAJI, (Member, IEEE)
Department of Sensor and Biomedical Technology, School of Electronics Engineering, Vellore Institute of Technology, Vellore 632014, India
Corresponding author: Debashis Maji (debashis.maji@vit.ac.in)

This work was supported by the Science and Engineering Research Board under the Department of Science and Technology (DST-SERB), India, for sponsoring the funds from Project Grant-DST SERB-File Number/ECR/2018/001295.

ABSTRACT Chronic wound care has always been a major challenge for healthcare professionals and is a significant public health crisis. Electrical stimulation (ES) therapy is an effective alternative treatment for chronic and acute dermal wounds by promoting electrotaxis of different types of cells during different stages of wound healing. In the present work, a simulation of guided electrotaxis through external ES was carried out using 2D and 3D finite element analysis of a wound model. Initial simulation work was performed using COMSOL Multiphysics 5.3®which highlighted the efficacy of micro-electrode arrays (MEAs) compared to the conventional two-electrode system. Further design optimization includes the incorporation of a gap between the electrode surface and wound bed to achieve an optimal EF gradient of ∼140-200 mV/mm at the wound periphery, along with reduced electrical spikes and uniform EF distribution for effective electrotaxis. This study also highlights strategies for fabricating a flexible and conformal aluminum thin-film MEA patch over a polydimethylsiloxane (PDMS) elastomer using the thermal evaporation technique through a stencil mask. A novel technique for stress-free self-release of the fabricated electrode was adopted using a polyvinyl alcohol (PVA) sacrificial layer to realize a crack-free electrically continuous patterned structure. Furthermore, an initial ES study over agar-based phantoms was also carried out, which gave promising results by faithfully reproducing input-applied signals. The present initial investigation could therefore be used to develop a wound-healing bandage that could accelerate wound healing through electrical stimulation.

INDEX TERMS Agar phantom study, electrical stimulation therapy, electro-taxis, micro-electrode array (MEAs), flexible MEA patch.

I. INTRODUCTION

Millions of people worldwide suffer from wounds caused by trauma or postsurgical healing complexities. The field of epidemiology of chronic wound care is very challenging. Inadequate wound care attention particularly when coupled with complex ailments such as diabetes mellitus, leprosy, severe burns, and venous ulcers, can lead to sepsis and bacteremia due to infections [1], [2], [3], [4]. As reported by Chandan et al. the medicare cost for ∼8.2 million people is about $96.8 billion for all kinds of wound care, including infection management and diabetic foot ulcer [5]. As per the National Institutes of Health's (NIH) report, the market for wound care devices could reach up to $22 billion by 2024 [5]. Moreover, severe injuries and wounds that cause serious damage to the epidermal layers of the skin inhibit the normal wound healing process involving homeostasis, inflammation, proliferation, and remodeling stages [6], [7], [8], demanding the need for the development of a smart wound care solution.

Wound care therapies can be broadly classified into active and passive types. Active therapy includes hyperbaric oxygen treatment (HBOT), ultrasonography (US), ultraviolet light (UV), negative pressure therapy (NPWT), and skin grafts. Passive therapy on the other hand involves the use

The associate editor coordinating the review of this manuscript and approving it for publication was Agustin Leobardo Herrera-May.

of antimicrobial agents, antiseptics, and antibiotics to control the spread of bacterial infections [9]. Irrespective of the above techniques, accelerated wound healing is highly beneficial not only in daily life but also in the chronic wound care regime [10]. Recently, the use of electrical stimulation (ES) as an active wound care practice that promotes accelerated healing has been adopted because of its various advantages over traditional wound care methods [11]. ES has been proposed as a therapeutic model of wound care for many decades and is reported to reduce wound size and expedite natural wound healing by triggering protein synthesis, enhancing cellular immunity, cell reproduction, cell migration, and angiogenesis by organizing blood capillary formation [12], [13], [14], [15].

Recently, ES has gained widespread attention due to rapid advancements in the understanding of the biological factors of wound healing. However, an inadequate optimization of this technology and its deployment as a usable patch limits its application by healthcare professionals. The human skin is considered a battery with an endogenous electrical field called transepithelial potential (TEP) [16]. This TEP is caused by the movement of Na^+ and Cl^- ions by Na^+/K^+ ATPase pumps through the cellular layers within the top of the stratum corneum and bottom of the dermis layer [15] and is typically in the range of 10∼60 mV [8], [16], [17]. When a wound is created, the TEP flows parallel to the epithelial layer, producing a short circuit near the wound area. This EF is called the current of injury, which directs the TEP toward the center of the wound, as shown in Fig. 1(a). L C Kloth suggested the wound EF gradient to be 140 mV/mm at the wound periphery, which gradually reduces to ∼10 mV/mm within 1–3 mm from the wound center [18] as shown in Fig. 1(b). McCaig et al. in their review article reported one of the earliest demonstration of injury current formation in the skin by Du Bois-Reymond where wounds formed over humans, guinea pigs and amphibians immediately developed a steady EF of ∼140 mV/mm and the injury currents poured out of the lesions [19]. Further, Nuccitelli et al. suggested that the EF formed at the site of injury was typically around 100∼200 mV/mm which decreased gradually towards the center [20].

Various groups worldwide have tried to use this ES technique for wound healing applications by developing smart micro-electrode array (MEA) patches [21], [22]. In this context, various commercially available electrical stimulation devices as mentioned below exist for wound healing. Houghton et al. reported a high voltage pulsed electrical wound healing device called Micro Z© which was used to treat chronic pressure ulcers [23] and involved wearing of an electroconductive sock coupled with a stimulation module. However, no definite ES test protocols were derived and its utility was more tuned towards the patient and caregiver skills. PosiFect RD™ by BIOFiSica (UK) Ltd and Procellera® by Vomaris, Inc., use metallic electrodes to cure chronic wounds [24]. However, they are very unconformable to wear because of their large size and rigidity thereby causing skin inflammation and psychological stress when used for a long time. Rivkah et al. reviewed WoundEL® as a micro current stimulator module for wound healing that provides pulsed direct current stimulation through patch electrodes [21] which are too large to wear and also affect the mobility of the patient while wearing it. Thus, the development of a skin-friendly patch conformal with the skin layer and causing minimal irritation along with standardized ES test protocols are of immediate need for effective deployment of the above patch. In this context, various research is also being carried out worldwide to address the above issues. Kai et al in 2017, developed a bio plaster containing a built-in enzymatic biofuel cell using carbon nanotube and bilirubin oxidase as electrodes for wound healing [25]. However, the plasters require to be replaced with new ones after every 12 hours to replenish the external EF generated by the biofuel cell as its activity diminishes. X F Wang et al. in 2021 developed a printed circuit-based electrical wound healing bandage by incorporating Vaseline–chitosan wet gauze beneath the circuit and stimulating electrodes over PI substrates [22] and was used for treating diabetic wounds. Very recently, C Wang et al. have developed a printed conductive hydrogel-based ePatch using silver nanowire which was experimented on rodents for electrical wound healing [26] and showed appreciable healing within 7 days for an 8 mm diameter wound.

Although the above studies demonstrate promising results, the use of complicated fabrication processes, repetitive patches, or incorporation of bulky electronic components will again hinder the long-term usage of these devices. In this context, although the use of multiple electrodes is beneficial, the complexity of their attachment over the skin surface, increased patient discomfort and decreased mobility have reduced the acceptance of this particular technology. Hence, the development of simple and flexible skin-friendly patches with proper arrangements of MEAs is highly desirable to study the electric field distribution around them for effective electrotaxis. In this regard, an initial simulation mimicking the naturally occurring endogenous electric field was carried out using COMSOL Multiphysics® software over an appropriately modeled wound bed, followed by the application of external EF stimulation through various MEA geometries to assist the same. This work also highlights the various fabrication steps involved in the realization of a simulated micro-electrode array (MEA) patch containing aluminum electrodes over a biocompatible and flexible polymer surface, namely, polydimethylsiloxane (PDMS). In addition, a novel stress-free release of patterned MEAs was also discussed, and preliminary test results of applied stimulation over phantom models were demonstrated to prove the efficacy of the developed patches.

II. SIMULATION WORK

The EF distribution within biological tissues and organs is highly complex. Anatomically skin has multiple layers and many sub-layers. The EF for such cases can be considered as a stationary process occurring homogenously in each layer under an applied DC potential, assuming the skin layers

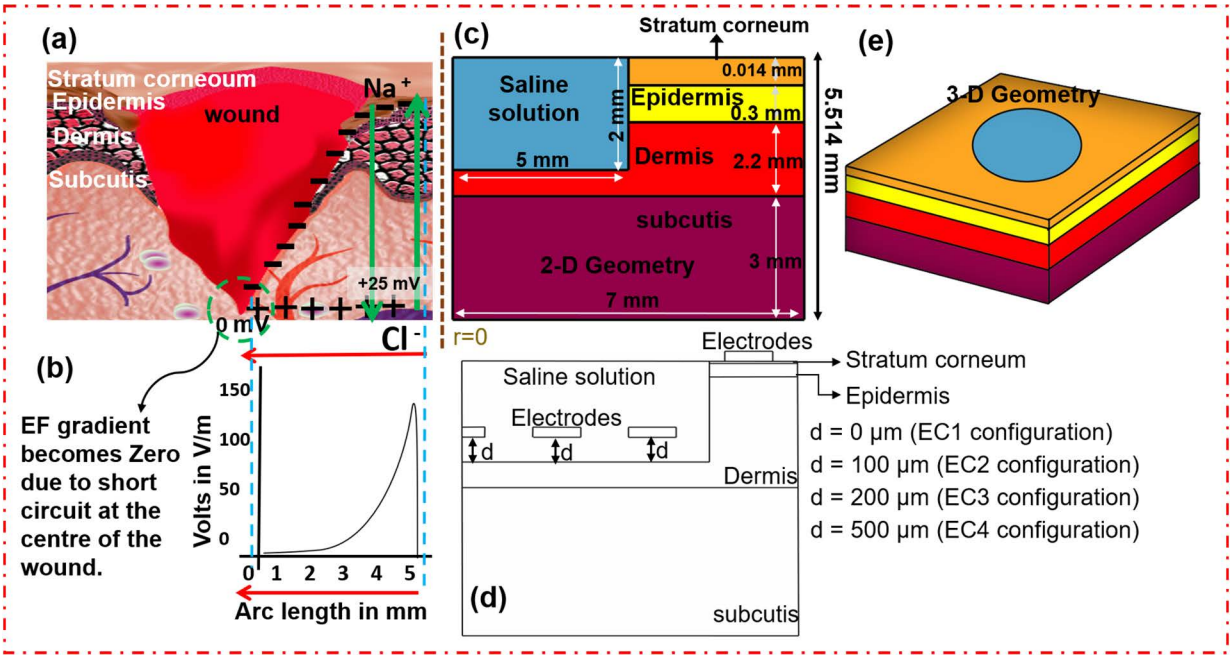

FIGURE 1. (a) Schematic representation of a wounded skin with basic skin layers showing the (b) EF gradient from the wound perimeter (∼150 mV/mm) to the centre of the wound (0 mv/mm). (c) 2D Geometry of the wound model with various skin layers and saline solution above the wound bed (not to scale) as per the modelled dimensions, (d)Denotes the electrode configurations (not to scale) (EC1-EC4) by a gap d between the electrode and wound bed and (e) 3D model of the same.

as isotropic conductors with discreet electrical parameters, relative permittivity (ε), and conductivity(σ). A 2D symmetry and 3D finite element modeling of the subcutaneous wound with different skin layers was simulated using COMSOL Multiphysics®5.3. Applied input electric potential (V) and boundary conditions were modeled as Dirichlet's boundary condition within the surface of skin tissue and exogenous stimulation electrodes.

A. TISSUE LAYER

In the present study, the skin structure has been modeled using only the most fundamental and phenomenal layers of epidermal skin namely stratum corneum, epidermis, dermis, and subcutis as shown in Fig. 1(a) and (c). The surface of the skin and wound has been assumed to be completely immersed in saline solution to enhance better electrical conductivity. The electrical conductivity and relative permittivity properties were assigned for each different skin layer [15], [27]. The numerous Na^+/K^+ pumps at the epithelium layer were also neglected with constant polarization throughout each layer, as the simulation only tries to optimize electrodes and their electric field distribution in the skin-electrode layer [28].

B. DESIGN OF 2D WOUND MODEL

Fig. 1(a) shows the schematic representation of the skin cross-section along with the formation of a wound at its center and the movement of the Na^+ and Cl^- ions through the ion channels rendering the top stratum corneum layer with negative potential and bottom dermal layer with positive potential.

TABLE 1. Material characteristics of the skin and wound.

	Conductivity (σ in Sm^{-1})	Relative Permittivity (ε_r)	Thickness (mm)
Stratum corneum	2×10^{-6}	5×10^2	0.014
Epidermis	0.026	10^6	0.3
Dermis	0.222	10^8	2.2
Subcutis	0.08	10^7	3.0
Saline	1.4	80	-

At the wound location the TEP short circuits and becomes 0 mV at the center of the wound. The endogenous EF is high near the wound periphery (∼140 mV/mm) and tends to gradually decrease to 0mV/mm when measured towards the center of the wound as observed schematically in Fig. 1(b).

The electrical stimulation model of the skin and the wound was designed and simulated using COMSOL Multiphysics® 5.3 as a 2D model. The skin geometry, the thickness of different layers, and their electrical properties like conductivity and relative permittivity were used from previous literature as highlighted by Sun et al. and detailed in Table 1 [15]. The endogenous EF was modeled to simulate and mimic the bio-electric field also known as the current of injury which is naturally present in the wounded skin surface. Fig. 1(c) shows the schematic illustration of one-half of a 2D cross-sectional skin model (not to scale), with the left margin being the line-symmetric, r=0 about the wound center. The total

skin thickness and cross-section half-width modeled in the 2D geometry was ∼5.514 mm and 7 mm respectively. The naturally occurring endogenous electric field of 40 mV/mm is simulated within the layer of the stratum corneum and epidermis. The skin was represented as a 2D rectangular patch having a circular wound filled with the saline solution having a half width of ∼5 mm and a depth of ∼2 mm from the top respectively. Each layer was defined with separate conductivity (σ) and permittivity (ε_r). The wound model was solved by finite element method using 6415 triangular elements, 463 edge elements and 12 vertex elements.

C. DESIGN OF ELECTRODE ARRAY

Finite element analysis is a reliable platform to apply appropriate electrical potential at the electrodes and observe the EF distribution. In our previous work [28], the effect of single and multiple electrode configurations of EF distribution over the wound bed was studied. The use of multiple electrodes as micro-electrode arrays (MEAs) demonstrated effective electrotaxis by enhancing the EF. Though the guided electrotaxis was achieved using the four-electrode system, the study showed the formation of a spiked electrical field near the electrode edges which could cause potential cell death and possibly disrupt the wound healing process [29], [30]

To resolve the above issue, a small gap was introduced between the MEA layer and the wound bed/dermis layer as shown in Fig. 1(d). This may be visualized as a more appropriate model as the MEAs would not be adhering physically to the wound bed using any adhesives but rather be covered by a thin layer of saline solution. The peripheral electrode was stimulated with a galvanic voltage of 40 mV, with the subsequent inner electrodes being stimulated with a decreasing potential of 30 mV and 20 mV respectively and the central one being grounded. Fig. 1(d) represents the various configurations that were tried showing the four electrodes as rectangular patches in 2D simulation. The dimensions of each 2D electrode were fixed to 1 mm in length and 200 μm in height. The four electrodes were placed at a distance of 0.5 mm, 1.5 mm, 3.5 mm, and 5.5 mm respectively from the center of the wound bed and were equally spaced with a separation of 1 mm between each electrode. The electrode at 5.5 mm was always positioned on the unwounded skin in all configurations to improve the movements of newly generated cells with gradient electric fields supporting the electrical wound stimulation process. Similarly, the central round electrode was fixed as the ground electrode in all simulations. Four different configurations (EC1, EC2, EC3, and EC4) were tested incorporating no gap and a gap of 100 μm, 200 μm and 500 μm between the MEA layer and the wound bed/dermis layer respectively as shown in Fig. 1(d). Expect the (EC1) configuration, others have saline solution filling the gaps between the wound bed and electrode.

D. 3D DESIGN OF THE WOUND BED AND SKIN

The four skin layers along with the wound were also designed in 3-D geometry as a square skin patch of ∼7 mm width and thickness of ∼5.5 mm having a cylindrical wound of ∼ 5 mm radius and 2.2 mm wound depth as shown in Fig. 1(e). The 3D model of it represents the electrodes as concentric rings having fixed radii of 0.5 mm, 1.5 mm, 3.5 mm, and 5.5 mm respectively from the center toward the periphery. All design settings were kept similar to that of the 2D model and the effective distribution of EF over a 3D wound bed region was simulated using this model.

III. FABRICATION OF MICRO-ELECTRODE ARRAYS (MEAs)

Fabrication of the micro-electrode array (MEA) patch for electrical stimulation was realized using the physical vapor deposition technique of aluminum over Polydimethylsiloxane (PDMS) substrate due to superior flexibility, high transparency, chemical inertness, high thermal stability, and good biocompatibility of PDMS towards such sub dermal studies [31]. A stencil mask technique was used for patterning the MEAs as highlighted below using aluminum thin film from Merck (Al thin wire of diameter 1 mm and ≥99.99% purity). A novel stress-free method of releasing the fabricated structures was employed by incorporating a PVA sacrificial layer below the PDMS substrate to release the samples spontaneously under water.

A. STENCIL MASK PREPARATION

The realization of a conformal electrode array patch was achieved using a stencil mask-assisted physical vapor disposition technique. Appropriate stencil masks were fabricated using the electron discharge machining (EDM) method over a thin stainless-steel sheet as discussed in [32]. The fabricated stencil mask was smoothly rubbed with a code 2000 emery sheet to dust off any residual particle contamination during the processing time. Thereafter, it was immersed in isopropyl alcohol and sonicated for 15 mins in a water bath to remove any finer impurities from the surface of the mask. As a final step of cleaning, the stencil was rinsed thoroughly in deionized (DI)water and kept over a hot plate to evaporate any solvents adhering to the stencil surface.

B. SYNTHESIS OF PVA SACRIFICIAL LAYER

Water soluble polyvinyl alcohol PVA from LOBA CHEMIE 9002-89-5 ADR was used as a sacrificial layer beneath the substrate to effortlessly release the final PDMS film from the underlying glass substrate without any stress. PVA aqueous solution was prepared by mixing 10 grams of PVA in 100 ml of boiling deionized water and mechanically stirring it until the solution turned homogenous and transparent without containing any undissolved lumps of PVA [33].

C. SUBSTRATE PREPARATION

Micro slides from HIMEDIA (premium quality BG004) were used as the base. Glass slides were cleaned with piranha solution followed by rinsing in DI water and drying in a hot oven at 200 °C for 30 min. A sacrificial layer of PVA was created by spin coating 10% PVA aqueous solution over the

pristine glass slide at 1000 rpm for 20 s using APEX IC INDIA NXG-P2 spin coater. The spin-coated samples were allowed to rest and then dried at 50° C for 2 hours. A uniform coating of polydimethylsiloxane (PDMS) from Sylgard 184 (Dow-Corning Corporation, USA) was thereafter given to make flexible free-standing polymeric substrates. PDMS polymer samples were prepared by mixing PDMS elastomer and curing agent in the ratio of 10:1 (w/w) followed by degassing to remove air bubbles. Approximately a 1 mm thick PDMS layer was coated uniformly over the PVA sacrificial layer and degassed to release any trapped bubbles. Finally, the samples were cured at 120° C for 2 hours to ensure complete polymerization.

D. SENSOR FABRICATION AND ITS RELEASE

Initially, the PDMS samples were exposed to oxygen plasma at 38 W using a plasma chamber (Harrick plasma - PDC -001-HP) for 30 s to render the surface hydrophilic and improve thin film adhesion [34]. Upon plasma treatment, the samples were immediately masked with pre-cleaned stainless steel stencil masks and placed inside the thermal evaporation chamber for metal deposition. Thereafter, thin film deposition was carried out with aluminum at a chamber pressure of 3×10^{-5} m-bar for 5 min. Finally, after deposition, the stencil was carefully removed from the PDMS top surface and the electrode pattern was immersed in 60° C deionized water with gentle mechanical stirring for the water to enable the dissolution of the PVA sacrificial layer. After about 35 min the PDMS-aluminum (PDMS-Al) MEA patch was observed to be floating over the top surface of the water indicating the complete dissolution of the PVA layer and subsequent release of the same thereafter. Finally, the released samples were dried on a hot plate for 30 min and silver conductive epoxy paste was used to take contacts from the bond pads using double enamel thin copper wire for further electrical study.

E. ELECTRICAL STIMULATION STUDY ON PHANTOMS

Phantoms are systems that physically emulate the properties of any living tissue. It has also been used in a variety of biomedical applications like ultrasound imaging [35], electrical impedance tomography [36], optical tomography [37], etc. This paper extends to developing a phantom model for galvanic electrical stimulation and observing the simulated EF through a phantom for the developed MEA patch. Agar-based material was used in the phantom to physically simulate biological living tissue. In the present case, the phantom model was prepared by first slowly mixing 100 gm of agar into 100 ml of DI water and heating at 60∼70° C without getting any lumps under continuous mechanical stirring. After complete dissolution, it was diluted with 500 ml of DI water containing 20% pre-heated NaCl solution. A drop of red food color was added just to look similar to the biological tissues. The mixture was then transferred to petri plates and refrigerated until it completely solidified into a gel. After complete gelation, the mould was released and used for phantom study.

The agar-based phantom was placed over the fabricated electrodes and the EF response was simulated similarly to the COMSOL simulations. After establishing proper connections, different voltage levels similar to the COMSOL simulation were generated in LabView and applied using NI-9264 analog output to the MEA patch. A phantom of ~ 6 mm thickness was placed over the patch and the output data was measured using a Keysight 3466A digital multimeter (DMM) in continuous trend chart mode.

IV. RESULTS AND DISCUSSION

Bio-mimicking of EF distribution similar to the endogenous EF was achieved and demonstrated a significant possibility of accelerated wound healing through effective electrotaxis. This work also extends to fabricating a thin film-based electrode patch for ES therapy highlighting initial test results of ES over a suitable phantom model.

A. 2D SIMULATION RESULTS

The natural endogenous EF was kept to be 40 mV within the top of the stratum corneum and bottom of the epidermis layer. The EF intensity near the edge of the wound was observed to be ∼140 mV/mm which was very close to the theoretical observations within the range of 40∼200 mV/mm [16], [18], [19], [20]. Fig. 2(a) exhibits clock-wise endogenous EF traveling inwards from the un-wounded periphery to the top of the wound bed which is helpful in normal wound healing. Fig. 2(b) shows the direction of EF displacement vectors or electric flux density lines within the layers of skin, wherein it was observed that the horizontal field lines were present near the periphery of the injury and became perpendicular near the center of the wound. Fig. 2(c) clearly shows the strength of the EF gradually decreasing from around 140 mV/mm at the periphery to almost zero at the center of the wound.

Natural wound healing observations depict that healing rates are always directed inwards from the wound periphery towards the center This observation may be attributed to the above simulation result which shows horizontal EF displacement lines only near the wound periphery, suggesting effective electrotaxis near there. Further, as the healing proceeds, the junction moves inwards and so do the horizontal EF displacement lines contributing to gradual electrotaxis in natural wound healing. In this context, the gradually perpendicular EF flow lines towards the wound bed thus may not effectively contribute to the electrotaxis process.

To study the effect of external EF on wound healing, a simulation was performed using 2, 3, and 4 electrodes. Fig. 3(a) shows the 2-electrode configuration with one ground electrode at the center of the wound bed and a positive electrode with 40 mV at the wound periphery. Fig. 3 (b) shows the normalized EF displacement vectors across the wound and Fig. 3(c) shows the proportional distribution of EF displacement vectors which is highly focused only towards the center of the wound bed. Further, the magnitude of the EF gradient starts from 750 mV/mm which is quite high and suddenly descends sharply at the wound edge which may

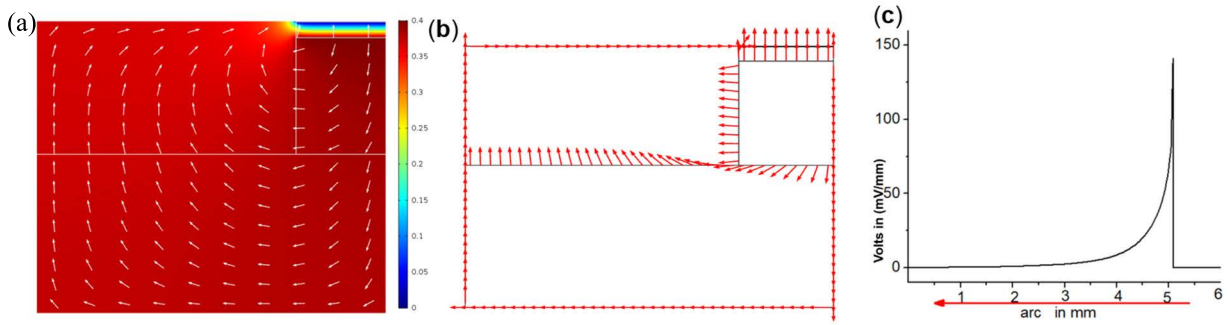

FIGURE 2. 2(a) 2-D distribution of endogenous EF, (b) direction of electric field displacement vector or electric flux density (c) the decreasing electric field gradient of the current of injury due to endogenous EF.

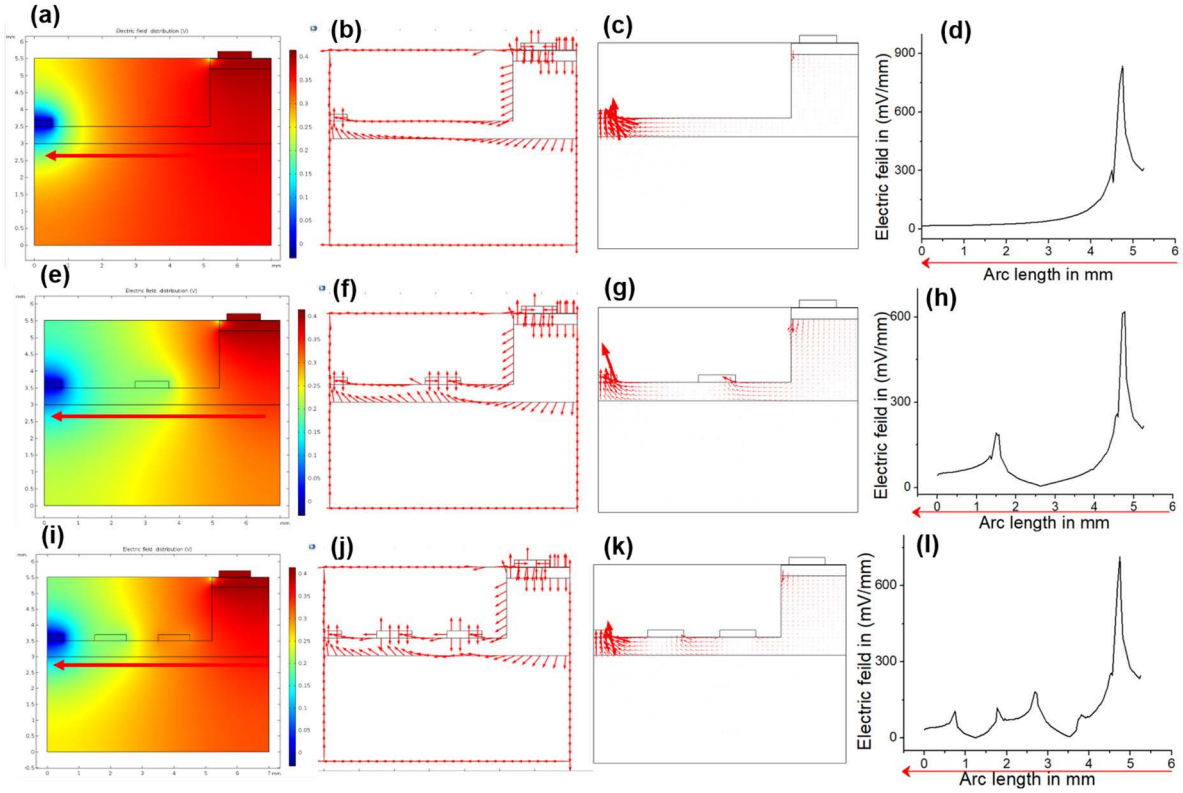

FIGURE 3. (a, e, i) shows the electric filed distribution plots for 2, 3 and 4 electrode system. (b, f, j) shows the normalized electric field displacement vectors of the respective configurations. (c, g, k) shows the proportional distribution of electric field displacement vectors and (d, h, l) shows the EF intensity across the wound towards the center for the above three configurations respectively.

not effectively aid the galvanotaxis process. Thus, another electrode was incorporated between the existing electrodes as shown in Fig. 3(e) which distributed the EF gradient across the entire wound region. It was observed that the incorporation of additional electrodes generates more field lines in the region between the wound periphery and its center as highlighted through the EF displacement vectors in Fig 3 (f-g). Fig. 3 (h) shows the EF gradients across the wound which also had an initial magnitude of ∼600 mV/mm and showed the incorporation of an additional spike near the middle electrode. To enhance the distribution of the EF gradient and direct the EF lines further toward the center, another electrode was incorporated. Fig. 3 (i, j, k) shows the color plot, normalized EF displacement vector, and proportional EF displacement vector respectively for the four-electrode configuration. This four-electrode configuration enhanced the displacement and distribution of the EF field across the wound, particularly in regions near the electrodes. Fig. 3(i) shows the EF gradient distribution, which again shows the presence of spikes along with an initial EF spike of ∼700 mV/mm which needs to be further considered. This increased spike in the EF gradient across the wound may cause cell death and tissue damage

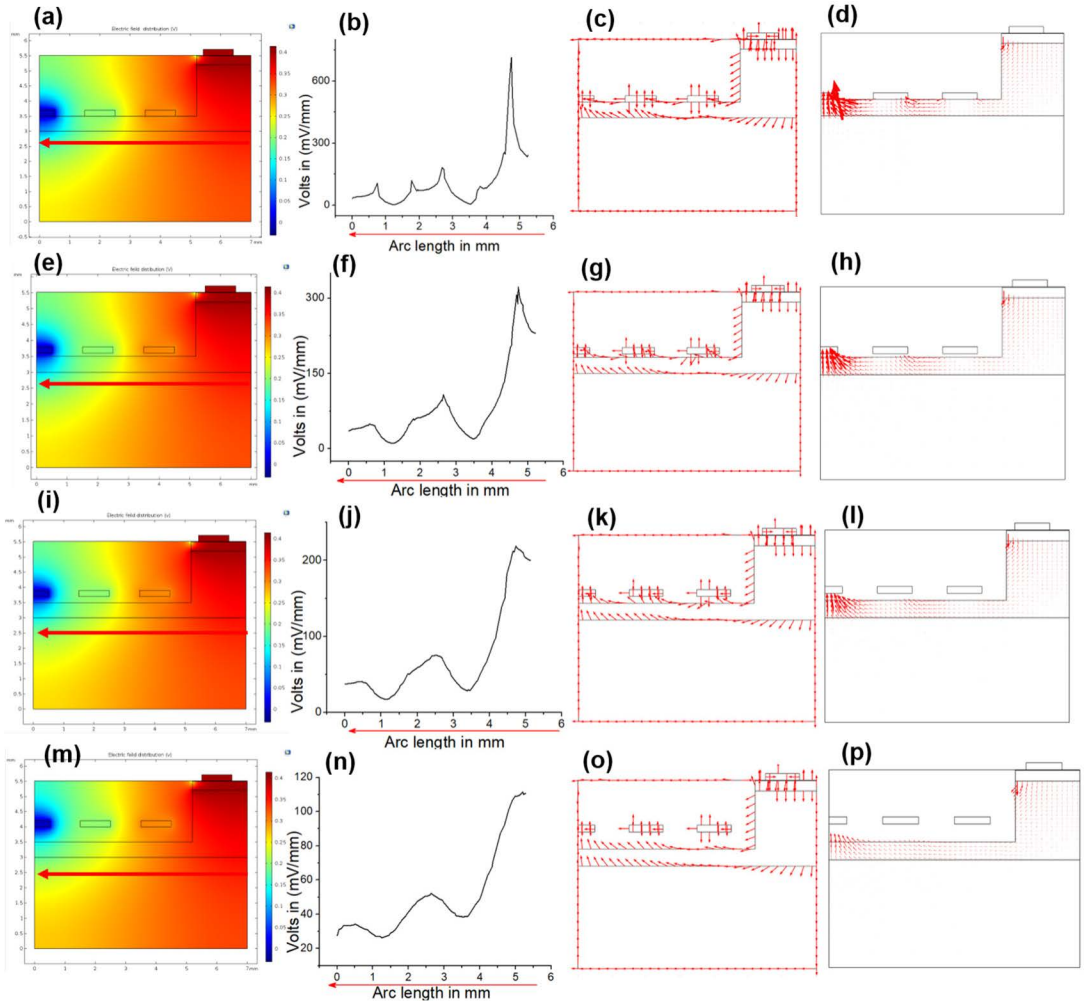

FIGURE 4. (a, e, i, m) shows the rainbow colour plot of EF distribution for the electrode configurations EC1-EC4 in the layers of the skin, (b, f, j, n) depicts the 1-D line graph of the electrode geometry showing the decreasing EF gradient from ∼600mV/mm to ∼140mV/mm with increased smoothness, (c, g, k, o) depicts the arrow line graph showing the EF directional flow in between the skin layers and the EF acting on the skin-wound surface with (d, h, I, p) denoting the proportional EF vectors for the above configurations respectively.

[29], [30] which may slow the wound healing rate. Hence, this four-electrode model was further explored to modify the placement of the electrodes to decrease the spiking voltage gradients and achieve a gradual decrease in the EF gradient across the wound. Fig. 4 shows the galvanic stimulation of the exogenous EF distributions of the EC1, EC2, EC3, and EC4 configurations for the four-electrode system. As mentioned earlier, the electrodes were placed over the wound region such that three of them were over the wound bed and one was over healthy skin at its periphery. The EC 1 configuration had four electrodes placed over the wound bed and unwounded skin surface, as described in the previous section which showed a high initial EF magnitude of ∼750 mV/mm at the wound periphery and voltage spikes across the wound center, as shown in Fig. 4(a-d). To eliminate these issues and decrease the EF gradient similar to the natural endogenous voltage, a small gap was introduced between the electrodes and the wound bed. In the EC2 configuration, electrodes were placed 100 μm above the wound bed, as shown in Fig. 4(e).

This modification in the placement of the electrodes decreased the initial EF gradient from ∼750 mV/mm to 320 mV/mm, as shown in Fig. 4(f). Fig. 4(g & h) show the normalized and proportional EF displacement vectors respectively across the wound and are observed to be more uniformly distributed as compared to the EC1 configuration. In the EC3 configuration, the gap between the electrode and the wound bed was further increased to 200 μm. Fig. 4(i) shows a rainbow color plot of the EF distribution of the EC3 configuration. This configuration further decreased the EF gradient from 320 to 200 mV/mm at the periphery, as shown in Fig. 4(j), and also showed a better smoothing effect of EF owing to the increased gap between the skin and wound bed. Fig. 4(k & l) shows the normalized and proportional EF displacement plots, respectively. Finally, the

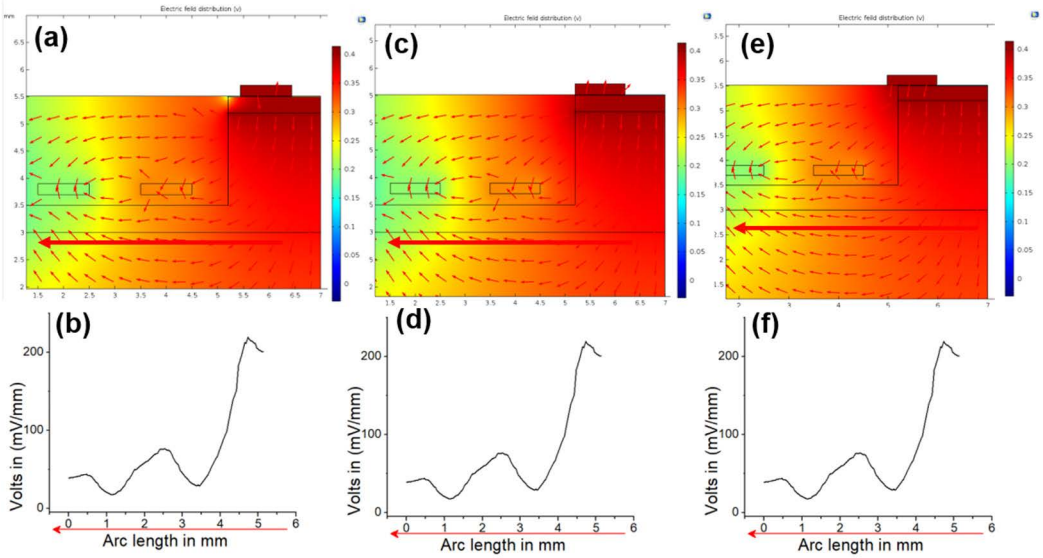

FIGURE 5. (a, c, e) shows magnified view of the EF distribution of the electrode- skin interface with relative displacement between the electrode and skin surface. (b, d, f) shows there is no change in the acting EF gradient on the skin even when there is a shift in their relative positioning.

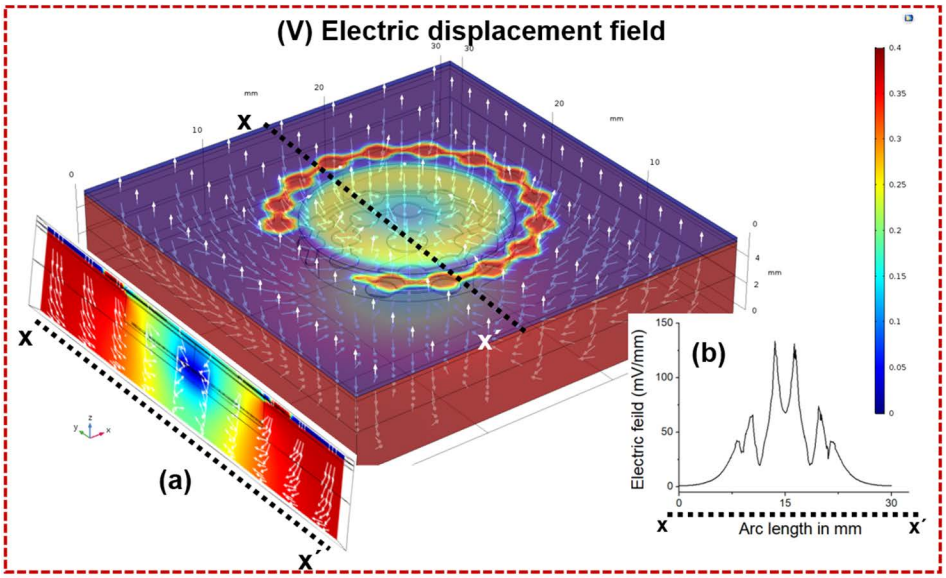

FIGURE 6. 3D distribution of the exogenous stimulation with directional electric field vectors travelling towards the centre of the wound. Inset (a) shows 2-D slice view across the centre of the wound highlighting EF arrows directed towards the top surface at the centre of the wound and inset (b) shows EF gradient across the centre of the wound (x-x′).

gap between the electrode and skin interface was further increased to 500μm as shown in EC4. This gap drastically regulates and distributes the EF gradient across the wound to $\sim$ 140 mV/mm, as shown in Fig. 4(n), which almost matches the naturally existing endogenous EF. Fig. 4(m) shows the color plot of the EC4 configuration. It was observed that the distribution of EF was almost uniform compared to all other electrode configurations. The normalized EF displacement vector also showed that the EF vectors were parallel to the wound surface near the wound edge and perpendicular only near the wound center, as shown in Fig. 4(o), similar to the endogenous EF displacement vectors shown in Fig. 3(c). The above simulation results indicate that the incorporation of a gap reduces the initial EF magnitude at the wound periphery, to almost 200 mV/mm to 140 mV/mm for electrode gaps of 200–500 μm. Furthermore, a uniform distribution of the EF displacement vectors was achieved between the electrode surface and the wound bed within this gap range. Thus,

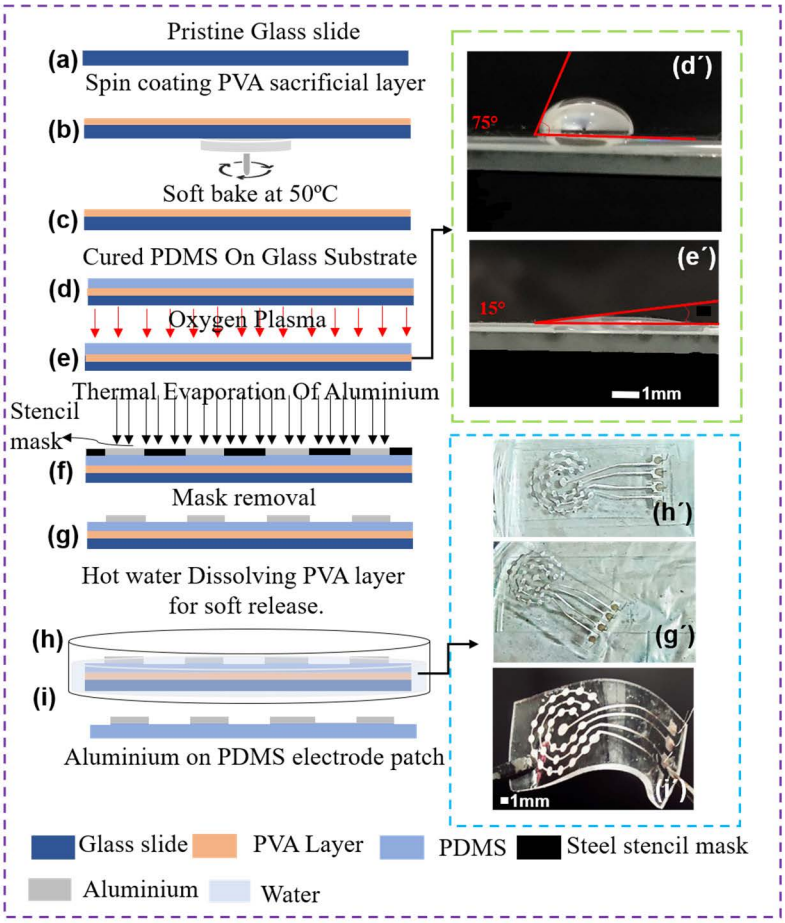

FIGURE 7. (a) Fabrication process steps for the MEA patch showing (a) pristine glass slide, (b) PVA spin coating layer, (c)soft baking PVA layer, (d) curing of PDMS elastomer over glass slides, (e) fixation of stencil mask over PDMS surface and exposure to oxygen plasma treatment, (f) thermal evaporation of aluminum, (g) removal of stencil mask and (h) removal of the sensor assembly from the glass support. (I) Fabricated flexible MEA patch over PDMS surface. Inset figures (d′ & e′) represents the contact angle of the water droplet formed over untreated PDMS surface 75° which decreased significantly 15° over the modified PDMS surface, indicating an increase in surface energy for effective thin-film adhesion.

we may conclude that for effective ES, a prominent gap of 200–500 μm may be observed during experimental studies. This may also be interpreted as a natural model because the electrode would never physically adhere to the wound bed and a minimal gap filled with a saline solution would always be present. However, care should be taken to ensure that the maximum gap does not exceed 500 μm, which otherwise would lead to reduced EF and ineffective implementation of ES.

The formation of a wound is generally not symmetrical or of any defined shape. Moreover, during fixation and with a gradual healing process, the position of the electrodes may change with respect to the underlying wound and/or the skin surface. Hence, a simulation study was conducted to demonstrate the effect of changes in EF on shifting electrode positions particularly for the peripheral one. Fig. 5(a), (c) and (e) shows the position of the outer electrode over the unwounded skin, near the wound edge, and halfway inside the wound respectively. As shown in Fig. 5, no significant changes were observed due to the above shift in the electrode positions in either the EF color plots or the gradient lines indicating that there is no effect on EF distribution due to a slight shift in the electrode positioning.

B. 3D WOUND MODEL SIMULATION

The 3D realization of the wound model, along with the effect of EF due to the 4-electrode configuration was modeled using COMSOL Multiphysics 5.3® as an extension of the 2D model. As discussed above, an optimized electrode configuration with electrodes at a distance of ∼200 μm above the wound surface was considered for the 3D model. Similar EF gradients were applied to electrodes in the EC4 configuration. Fig. 6 shows the 3D wound model indicating the directional

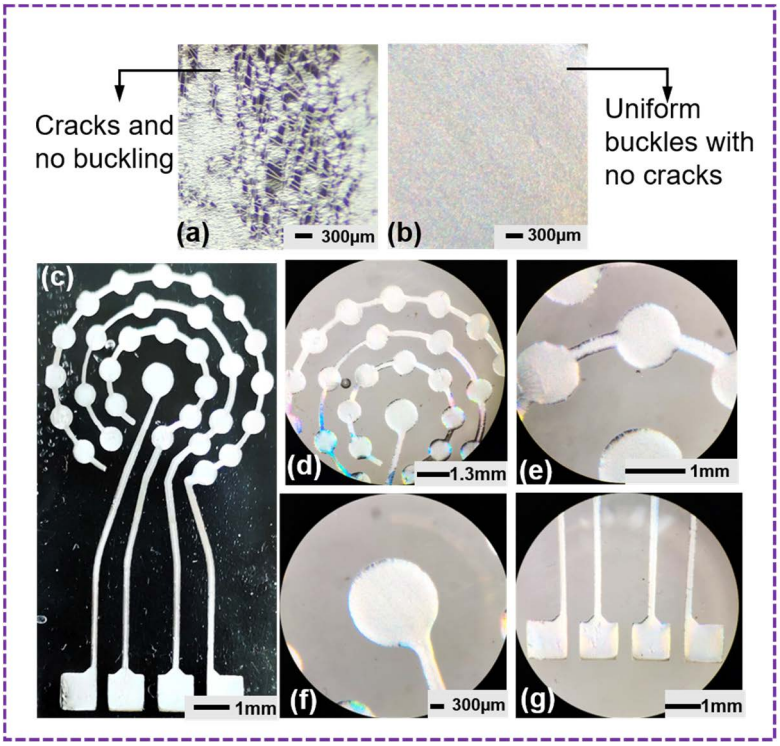

FIGURE 8. (a) Micro-cracks observed over aluminum surface after manual peeling off of the elastomeric patch post patterning and (b) formation of fine buckles with no cracks after stress free release of the samples under water, (c) microphotograph of the complete ES patch (i.e.) showing the circular stimulating electrodes in three concentric rings and attached to the connecting bond pads with magnified view of the (d, e) stimulating electrodes, (f) central ground electrode and (g) contact pads for electrical connections with the stimulation circuits.

flow of the EF with the white arrows pointing outwards (over the top skin surface) and inwards (within the wound) assisting the electrotaxis process. Inset A shows the 2D slice view of the EF displacement vectors across the wound cross-section (represented by the line x-x') and inset B shows the EF line graph observed for the same. EF was observed to be similar to the 2D simulation results of Fig. 4(o). The above 3D simulation also ensures a smoothened EF distribution with EF flow lines directed towards the center of the wound bed throughout its bulk thereby causing guided electrotaxis for the promotion of effective wound healing.

C. FABRICATION OF MEAs

In this study, thin films and MEAs were fabricated using a thermal evaporation technique. As illustrated in Fig. 7, the pristine glass slide (a), was spin-coated with a 10% PVA aqueous solution (b) to remove any moisture, creating a PVA sacrificial layer that was soft-baked at 55° C (c). The PDMS mix was poured over it to a thickness of ∼1 mm (d), and after complete polymerization, it was exposed to oxygen plasma for 30 s (e) to render the surface hydrophilic. Fig. 7 (d′ 1 & e′ 1) shows micrographs of 20 μl water droplets over the PDMS samples before and after the oxygen plasma treatment indicating hydrophilicity of the same post-surface modification. Thereafter, the stencil mask was aligned over the PDMS surface and thermal evaporation of aluminum was carried out (f). Subsequently, the mask was carefully removed (g), and the patterned sample was immersed in hot water to dissolve the PVA sacrificial layer (h). Finally, after dissolving the PVA layer, PDMS-Al MEAs was softly released from the glass substrate (i) for further electrical studies.

D. MICROSCOPIC OBSERVATION OF FABRICATED FLEXIBLE MEAs

Fig. 8(a) shows the formation of stress-induced cracks over the patterned aluminum surface when directly peeled off from the bottom glass substrate without any sacrificial layer. The structures demonstrated no electrical continuity and were unsuitable for further studies. On the other hand, when a hot water-soluble PVA sacrificial layer was incorporated beneath the PDMS elastomer, warm water gradually seeped between the PDMS and glass layers, dissolving the PVA within it, thereafter softly releasing the PDMS-Al MEAs from the glass surface as shown in Fig. 7(h′). Microscopic observation of these stress-free released MEAs revealed the presence of random wrinkles or buckles of aluminum metal over the entire PDMS surface as shown in Fig. 8(b) along with good electrical continuity within the patterns. Fig. 8(c) shows the completely fabricated MEA electrodes with three layers of

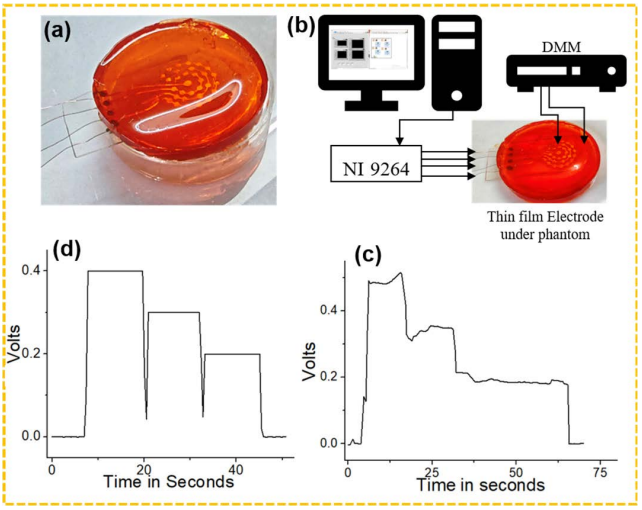

FIGURE 9. (a) shows the phantom placed over the fabricated electrode, (b) setup of the stimulation and data acquistition. (c) EF measurment through the phantom on the concentric ring surface. (d) EF measured without phantom.

concentric electrodes surrounding the central ground electrode. The diameter of each electrode was 1 mm with a 250 μm width interconnecting line between each electrode pair. Fig. 8(d-g) shows micrographs of various parts of the fabricated MEAs under different magnifications.

E. PHANTOM STUDY

An initial EF study was conducted over a phantom having a thickness of approximately 6 mm, which was placed over the fabricated MEA patch, as shown in Fig. 9(a). Silver conductive epoxy paste was used to take contacts from the bond pads of the MEA patch using double enamel thin copper wire. The fabricated electrode was placed over an agar-based phantom, and the EF response was simulated like the COMSOL simulations using a NI-9264 analog output module connected to the copper wires of the MEA patch. The output data were acquired simultaneously using a Keysight 3466A DMM, as shown in Fig. 9(b). The EF measurements were performed with and without the phantom. Fig. 9(c) shows the EF measurements over the skin phantom surface. The central electrode was maintained at a zero potential, as indicated in the simulation study.

Measurements were obtained for each concentric electrode layer with respect to the central ground electrode by manually touching the electrode surface with the DMM leads. The obtained graph shows an output electrical potential of 0.49 ± 0.019 V, 0.34 ± 0.013 V, and 0.19 ± 0.007 V for the three-electrode layers respectively over a phantom as compared to 0.4 V, 0.3 V, and 0.2 V for the same without any phantom as shown in Fig. 9(d). Which were the same as that at the input end.

Thus, this control experiment was used to confirm the electrical continuity of the fabricated structures and ascertain the output voltage differences in the presence of a phantom layer during the actual study.

V. CONCLUSION

The present study was an attempt to visualize the role of endogenous EF during the onset of wound healing through simulation studies, and mimic the same through external EF (electrical stimulation via MEAs) to enhance the healing rate. Various electrode configurations were simulated to determine the proper distribution of the EF over the wound bed. For effective electrotaxis, a minimum of four electrodes (in the 2D model) were necessary, with three positioned over the wound bed and the fourth near the periphery of the wound. Furthermore, the initial simulation results demonstrated spikes in EF when the MEAs were placed directly over the wound surface. Hence, a small gap filled with saline solution was introduced between the electrode and the wound interface which was optimized to $\sim$200 μm–500 μm, to obtain a uniform distribution of the EF displacement vectors with smoothed spikes and an initial EF gradient between 140 – 200 mV/mm at the wound periphery. The presence of this gap may also be perceived as the natural separation of the MEA bandage structure over the wound region. Furthermore, it was also observed that there was no effect on the EF distribution, even due to a shift in the electrode positioning during animal handling, indicating the ruggedness of the present sensor patch. This study also highlights the initial fabrication of the above-designed MEA patch over a biocompatible PDMS elastomer with aluminum-based micro-electrodes using the stencil mask technique. A novel stress-free self-release technique of the patterned MEAs was realized using a PVA sacrificial layer between the sensor and bottom glass. The fabricated sensors exhibited good electrical continuity without cracks. Further studies on the electrical responses of the applied ES over agar-gel-based phantoms were performed using a data acquisition system that gave promising results by faithfully reproducing the input applied signals. These initial studies highlight significantly the efficacy of the present system and its potential application as a smart wound healing bandage for its accelerated healing through ES therapy.

ACKNOWLEDGMENT

The authors are grateful to the Science and Engineering Research Board under the Department of Science and Technology (DST-SERB), India, for sponsoring the funds from the project grant DST SERB: File Number/ECR/2018/001295. They also acknowledge the support of DST-FIST supported MEMS and Chemical Sensors Lab (SR/FST/ETI-015/2011), VIT Vellore and MEMS Design Lab, VIT Vellore for extending its fabrication and designing facilities for carrying out this research work.

REFERENCES

[1] Y. Xi, J. Ge, M. Wang, M. Chen, W. Niu, W. Cheng, Y. Xue, C. Lin, and B. Lei, "Bioactive anti-inflammatory, antibacterial, antioxidative silicon-based nanofibrous dressing enables cutaneous tumor photothermo-chemo therapy and infection-induced wound healing," *ACS Nano*, vol. 14, no. 3, pp. 2904–2916, Mar. 2020.

[2] R. G. Frykberg and J. Banks, "Challenges in the treatment of chronic wounds," *Adv. Wound Care*, vol. 4, no. 9, pp. 560–582, Sep. 2015.

[3] N. Mookherjee, M. A. Anderson, H. P. Haagsman, and D. J. Davidson, "Antimicrobial host defence peptides: Functions and clinical potential," *Nature Rev. Drug Discovery*, vol. 19, no. 5, pp. 311–332, May 2020.
[4] P. Mostafalu, A. Tamayol, R. Rahimi, M. Ochoa, A. Khalilpour, G. Kiaee, I. K. Yazdi, S. Bagherifard, M. R. Dokmeci, B. Ziaie, S. R. Sonkusale, and A. Khademhosseini, "Smart bandage for monitoring and treatment of chronic wounds," *Small*, vol. 14, no. 33, Aug. 2018, Art. no. 1703509.
[5] C. K. Sen, "Human wounds and its burden: An updated compendium of estimates," *Adv. Wound Care*, vol. 8, no. 2, pp. 39–48, Feb. 2019.
[6] S. A. Eming, P. Martin, and M. Tomic-Canic, "Wound repair and regeneration: Mechanisms, signaling, and translation," *Sci. Translational Med.*, vol. 6, no. 265, p. 265, Dec. 2014.
[7] B. K. Sun, Z. Siprashvili, and P. A. Khavari, "Advances in skin grafting and treatment of cutaneous wounds," *Science*, vol. 346, no. 6212, pp. 941–945, Nov. 2014.
[8] J. Hunckler and A. De Mel, "A current affair: Electrotherapy in wound healing," *J. Multidisciplinary Healthcare*, vol. 10, p. 179, Jan. 2017.
[9] S. Finnegan and S. L. Percival, "EDTA: An antimicrobial and antibiofilm agent for use in wound care," *Adv. Wound Care*, vol. 4, no. 7, pp. 415–421, Jul. 2015.
[10] R. Luo, J. Dai, J. Zhang, and Z. Li, "Accelerated skin wound healing by electrical stimulation," *Adv. Healthcare Mater.*, vol. 10, no. 16, Aug. 2021, Art. no. 2100557.
[11] G. Thakral, J. LaFontaine, B. Najafi, T. K. Talal, P. Kim, and L. A. Lavery, "Electrical stimulation to accelerate wound healing," *Diabetic Foot Ankle*, vol. 4, no. 1, p. 22081, Jan. 2013.
[12] S. Ud-Din and A. Bayat, "Electrical stimulation and cutaneous wound healing: A review of clinical evidence," *Healthcare*, vol. 2, no. 4, pp. 445–467, Oct. 2014.
[13] S. Ud-Din, A. Sebastian, P. Giddings, J. Colthurst, S. Whiteside, J. Morris, R. Nuccitelli, C. Pullar, M. Baguneid, and A. Bayat, "Angiogenesis is induced and wound size is reduced by electrical stimulation in an acute wound healing model in human skin," *PLoS ONE*, vol. 10, no. 4, Apr. 2015, Art. no. e0124502.
[14] C. Chen, X. Bai, Y. Ding, and I.-S. Lee, "Electrical stimulation as a novel tool for regulating cell behavior in tissue engineering," *Biomaterials Res.*, vol. 23, no. 1, pp. 1–12, Dec. 2019.
[15] Y.-S. Sun, "Electrical stimulation for wound-healing: Simulation on the effect of electrode configurations," *BioMed Res. Int.*, vol. 2017, pp. 1–9, Apr. 2017.
[16] I. S. Foulds and A. T. Barker, "Human skin battery potentials and their possible role in wound healing," *Brit. J. Dermatol.*, vol. 109, no. 5, pp. 515–522, Nov. 1983.
[17] M. Zhao, B. Song, J. Pu, T. Wada, B. Reid, G. Tai, F. Wang, A. Guo, P. Walczysko, Y. Gu, and T. Sasaki, "Electrical signals control wound healing through phosphatidylinositol-3-OH kinase-γ and PTEN," *Nature*, vol. 442, pp. 457–460, Jul. 2006.
[18] L. C. Kloth, "Electrical stimulation technologies for wound healing," *Adv. Wound Care*, vol. 3, no. 2, pp. 81–90, Feb. 2014.
[19] C. D. McCaig, A. M. Rajnicek, B. Song, and M. Zhao, "Controlling cell behavior electrically: Current views and future potential," *Physiol. Rev.*, vol. 85, no. 3, pp. 943–978, Jul. 2005.
[20] R. Nuccitelli, P. Nuccitelli, C. Li, S. Narsing, D. M. Pariser, and K. Lui, "The electric field near human skin wounds declines with age and provides a noninvasive indicator of wound healing," *Wound Repair Regeneration*, vol. 19, no. 5, pp. 645–655, Sep. 2011.
[21] R. R. Isseroff and S. E. Dahle, "Electrical stimulation therapy and wound healing: Where are we now?" *Adv. Wound Care*, vol. 1, no. 6, pp. 238–243, Dec. 2012.
[22] X.-F. Wang, M.-L. Li, Q.-Q. Fang, W.-Y. Zhao, D. Lou, Y.-Y. Hu, J. Chen, X.-Z. Wang, and W.-Q. Tan, "Flexible electrical stimulation device with Chitosan-Vaseline dressing accelerates wound healing in diabetes," *Bioactive Mater.*, vol. 6, no. 1, pp. 230–243, Jan. 2021.
[23] P. E. Houghton, K. E. Campbell, C. H. Fraser, C. Harris, D. H. Keast, P. J. Potter, K. C. Hayes, and M. G. Woodbury, "Electrical stimulation therapy increases rate of healing of pressure ulcers in community-dwelling people with spinal cord injury," *Arch. Phys. Med. Rehabil.*, vol. 91, no. 5, pp. 669–678, May 2010.
[24] M. Ashrafi, T. Alonso-Rasgado, M. Baguneid, and A. Bayat, "The efficacy of electrical stimulation in experimentally induced cutaneous wounds in animals," *Veterinary Dermatol.*, vol. 27, p. 235, Aug. 2016.
[25] H. Kai, T. Yamauchi, Y. Ogawa, A. Tsubota, T. Magome, T. Miyake, K. Yamasaki, and M. Nishizawa, "Accelerated wound healing on skin by electrical stimulation with a bioelectric plaster," *Adv. Healthcare Mater.*, vol. 6, no. 22, Nov. 2017, Art. no. 1700465.
[26] C. Wang, X. Jiang, H. J. Kim, S. Zhang, X. Zhou, Y. Chen, H. Ling, Y. Xue, Z. Chen, M. Qu, and L. Ren, "Flexible patch with printable and antibacterial conductive hydrogel electrodes for accelerated wound healing," *Biomaterials*, vol. 285, Jun. 2022, Art. no. 121479.
[27] D. Semrov, R. Karba, and V. Valencic, "DC electrical stimulation for chronic wound healing enhancement. Part 2. Parameter determination by numerical modelling," *Bioelectrochemistry Bioenergetics*, vol. 43, pp. 271–278, Jan. 1997.
[28] G. H. Gnanasambanthan and D. Maji, "Effect on electrode configuration in electrical wound healing," *Mater. Today, Proc.*, vol. 63, pp. 382–386, Mar. 2022.
[29] T. B. Napotnik, T. Polajžer, and D. Miklavčič, "Cell death due to electroporation—A review," *Bioelectrochemistry*, vol. 141, Oct. 2021, Art. no. 107871.
[30] O. N. Pakhomova, B. W. Gregory, I. Semenov, and A. G. Pakhomov, "Two modes of cell death caused by exposure to nanosecond pulsed electric field," *PLoS ONE*, vol. 8, no. 7, Jul. 2013, Art. no. e70278.
[31] I. Miranda, A. Souza, P. Sousa, J. Ribeiro, E. M. S. Castanheira, R. Lima, and G. Minas, "Properties and applications of PDMS for biomedical engineering: A review," *J. Funct. Biomaterials*, vol. 13, no. 1, p. 2, Dec. 2021.
[32] H. Gnanasambanthan and D. Maji, "Reusable thin stainless steel shadow mask fabrication using electron discharge machining," in *Proc. IEEE 7th Int. Conf. Converg. Technol. (ICT)*, Apr. 2022, pp. 1–4.
[33] D. Maji, D. Das, J. Wala, and S. Das, "Buckling assisted and lithographically micropatterned fully flexible sensors for conformal integration applications," *Sci. Rep.*, vol. 5, pp. 1–16, Dec. 2015.
[34] D. Maji, S. K. Lahiri, and S. Das, "Study of hydrophilicity and stability of chemically modified PDMS surface using piranha and KOH solution," *Surf. Interface Anal.*, vol. 44, no. 1, pp. 62–69, Jan. 2012.
[35] K. Nightingale, M. Palmeri, and G. Trahey, "Analysis of contrast in images generated with transient acoustic radiation force," *Ultrasound Med. Biol.*, vol. 32, no. 1, pp. 61–72, Jan. 2006.
[36] T. J. Kao, G. J. Saulnier, D. Isaacson, T. L. Szabo, and J. C. Newell, "A versatile high-permittivity phantom for EIT," *IEEE Trans. Biomed. Eng.*, vol. 55, no. 11, pp. 2601–2607, Nov. 2008.
[37] R. Patra and P. K. Dutta, "Contrast improvement of continuous wave diffuse optical tomography reconstruction by hybrid approach using least square and genetic algorithm," *J. Biomed. Opt.*, vol. 20, Jul. 2015, Art. no. 075009.

G. HARISH GNANASAMBANTHAN received the B.E. degree in electronics and communication from the Aalim Muhammed Salegh College of Engineering, India, in 2017, and the M.Tech. degree in biomedical engineering from the Vellore Institute of Technology (VIT), India, in 2019, where he is currently pursuing the Ph.D. degree in flexible electronics with the School of Electronics Engineering (SENSE). His research interests include flexible polymeric electrode fabrication, printed electronics, surface modification, and flexible sensors.

DEBASHIS MAJI (Member, IEEE) received the M.Tech. degree in sensor system technology from the Vellore Institute of Technology (VIT), Vellore, India, and the Ph.D. degree in the interdisciplinary area of bioMEMS and flexible sensors from the School of Medical Science and Technology, IIT Kharagpur. He is currently a Senior Assistant Professor with the Department of Sensor and Biomedical Technology, School of Electronics Engineering (SENSE), VIT. His research interests include the design and fabrication of thin and thick film-based flexible biosensors for wearable applications, bioMEMS, and microfluidic biochips for disease diagnosis.